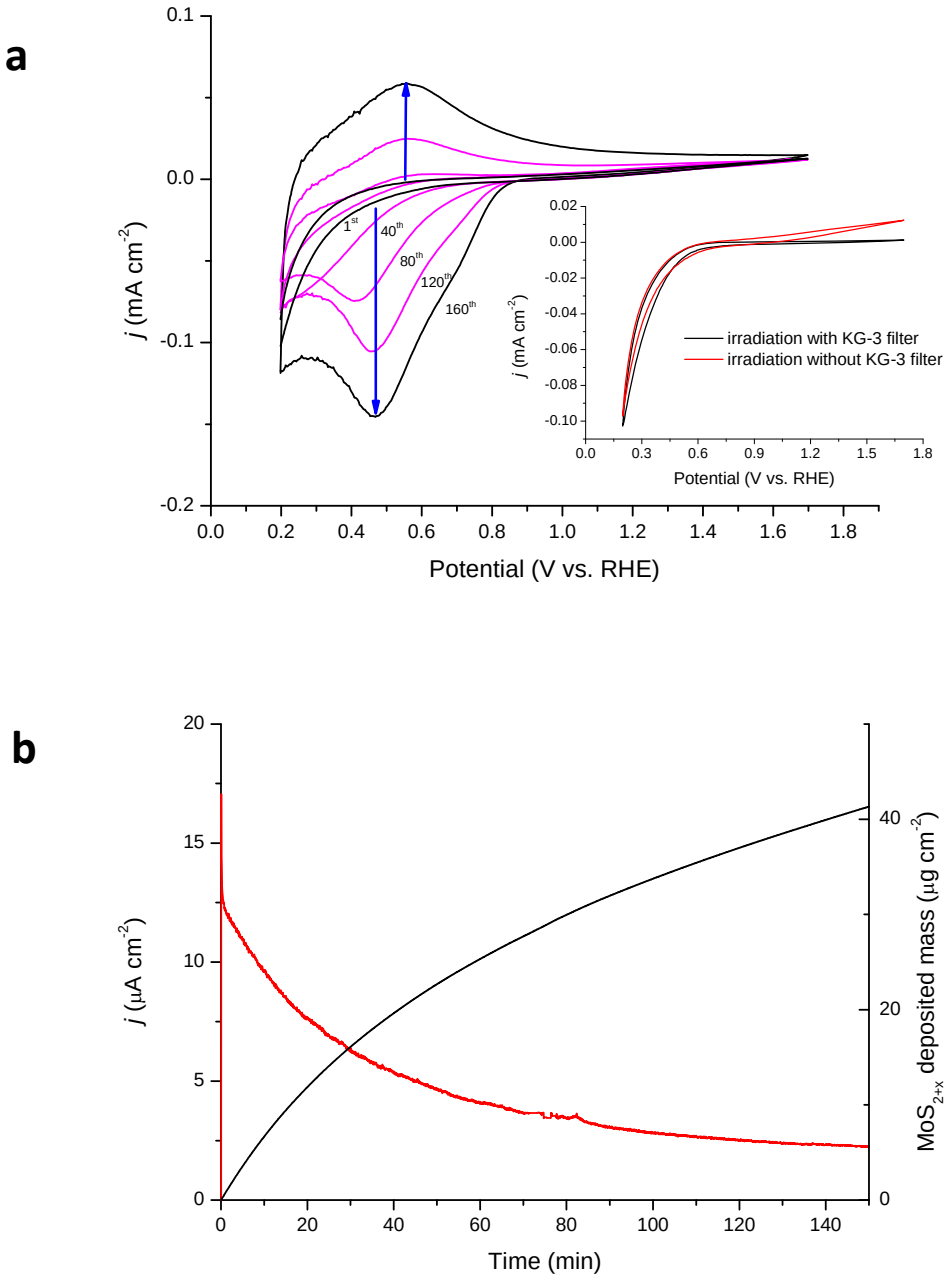

Supplementary Figure 1. MoS_{2+x} photoelectrodeposition. (a) Cyclic voltammetry deposition. Lines show scans 1 to 160 every 40 scans. The first and last scans are shown in black and the 40th, 80th and 120th scans are shown in pink. The chemical reactions related to the oxidative and reductive peaks and the film growth have been previously described by us for MoS_{2+x} electrodeposition on various conductive substrates.[20] Inset: photocurrent dependence on KG-3 filter presence. **(b)** Constant anodic deposition at 1.7 V vs. RHE. Deposited MoS_{2+x} mass was calculated from current density assuming a two electron oxidation process and a molecular weight of 160 g/mol for MoS_2.[20]

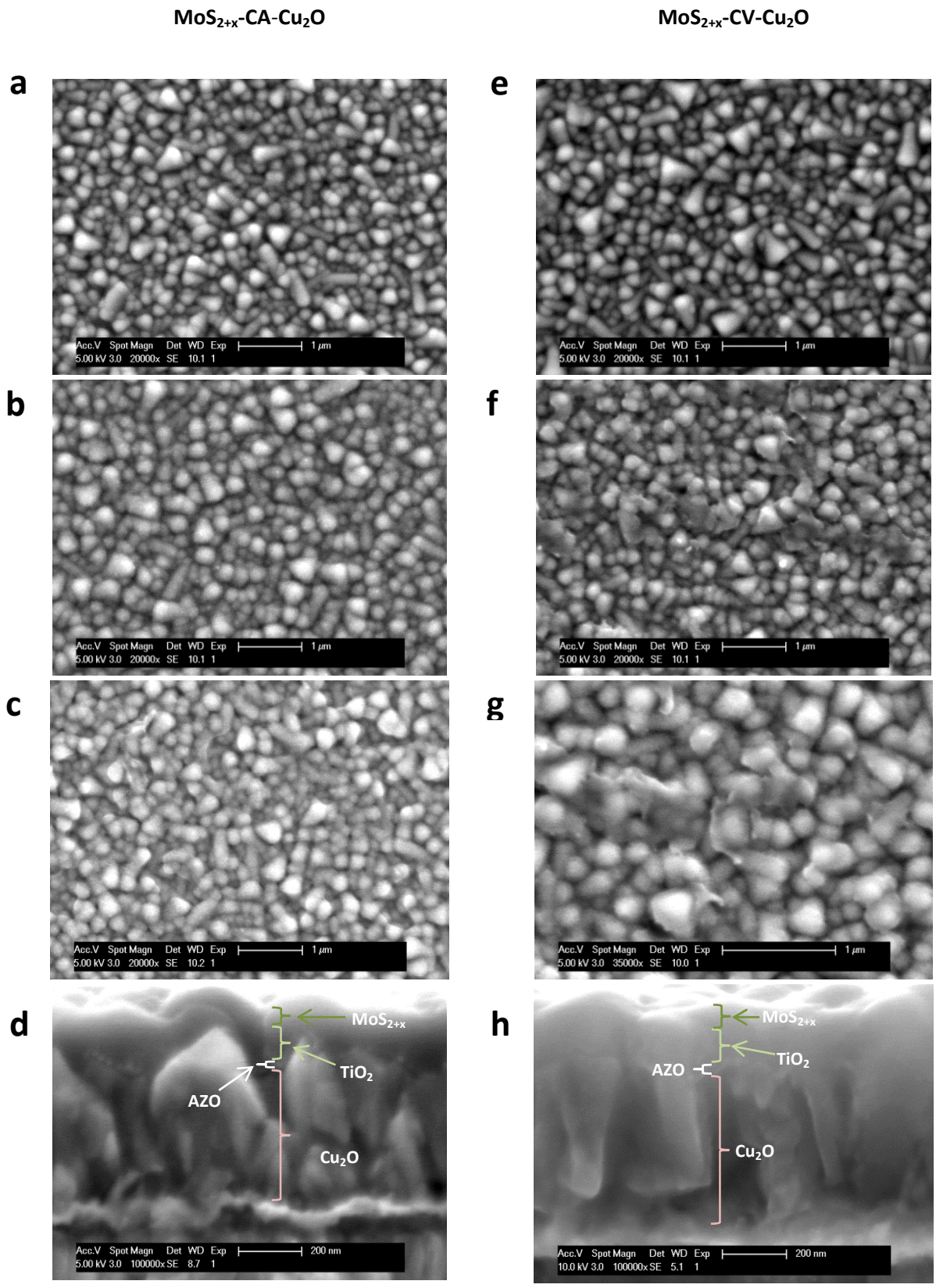

Supplementary Figure 2. MoS_{2+x}-Cu_2O photocathode SEM images. Surface protected Cu_2O photocathodes with MoS_{2+x} catalyst deposited by constant anodic potential (a-d) and by cyclic voltammetry (e-h). Photocathodes **(a,e)** before and **(b,f)** after deposition of HER catalyst. **(c,g)** Photocathodes after activation of the MoS_{2+x} catalyst film for hydrogen evolution during 1 h at pH 1.0 and **(d,h)** cross section of photocathodes in figures (c) and (g), respectively.

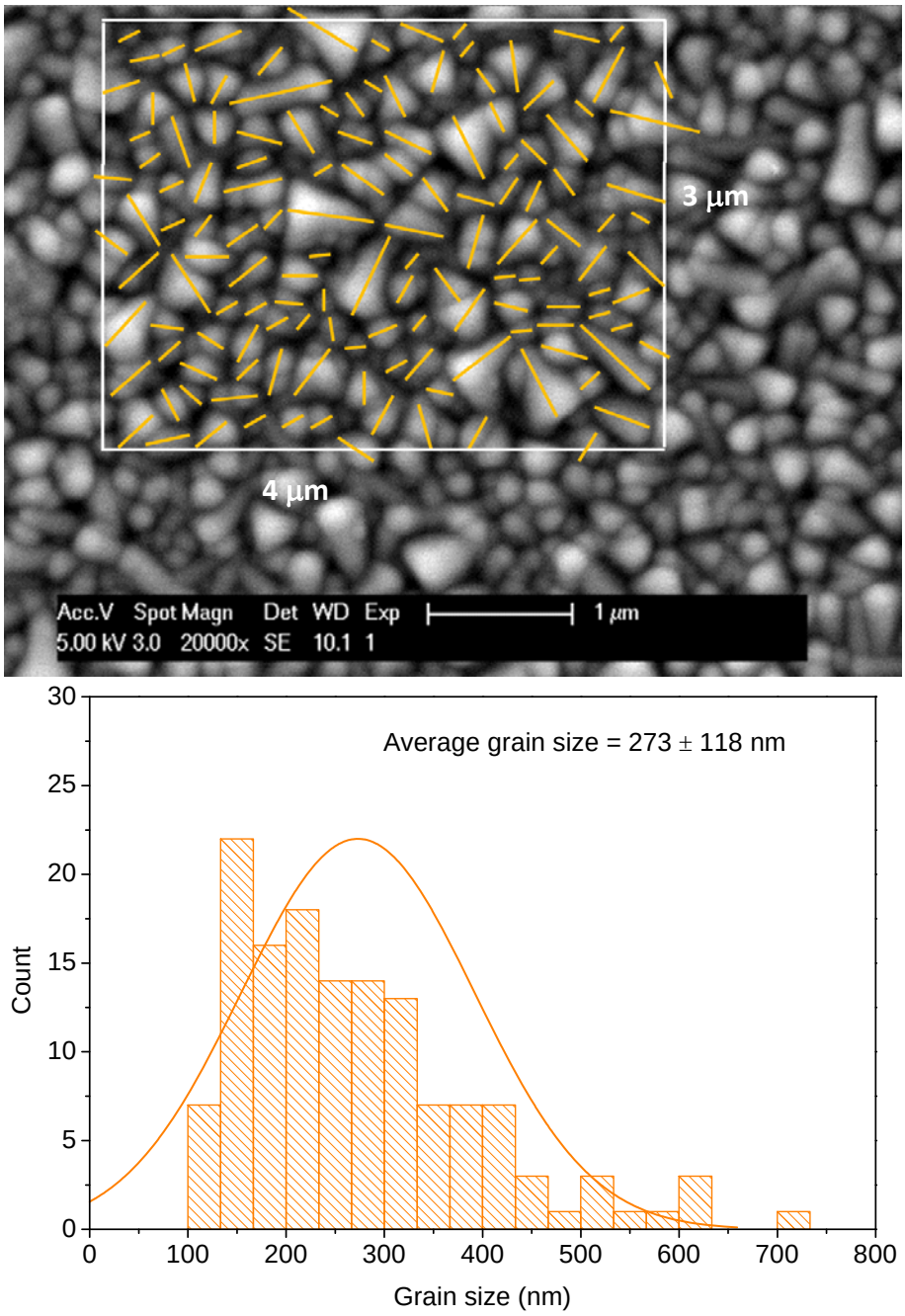

Supplementary Figure 3. Grain size distribution of the surface protected-Cu_2O photocathode before HER catalyst deposition. Average size determined for 138 grains in the representative area of 12 μm^2 indicated in the SEM image. Orange lines show the longest diagonal that can be traced for a grain. The sum of the squared values for the grain size gives 12.2 μm^2.

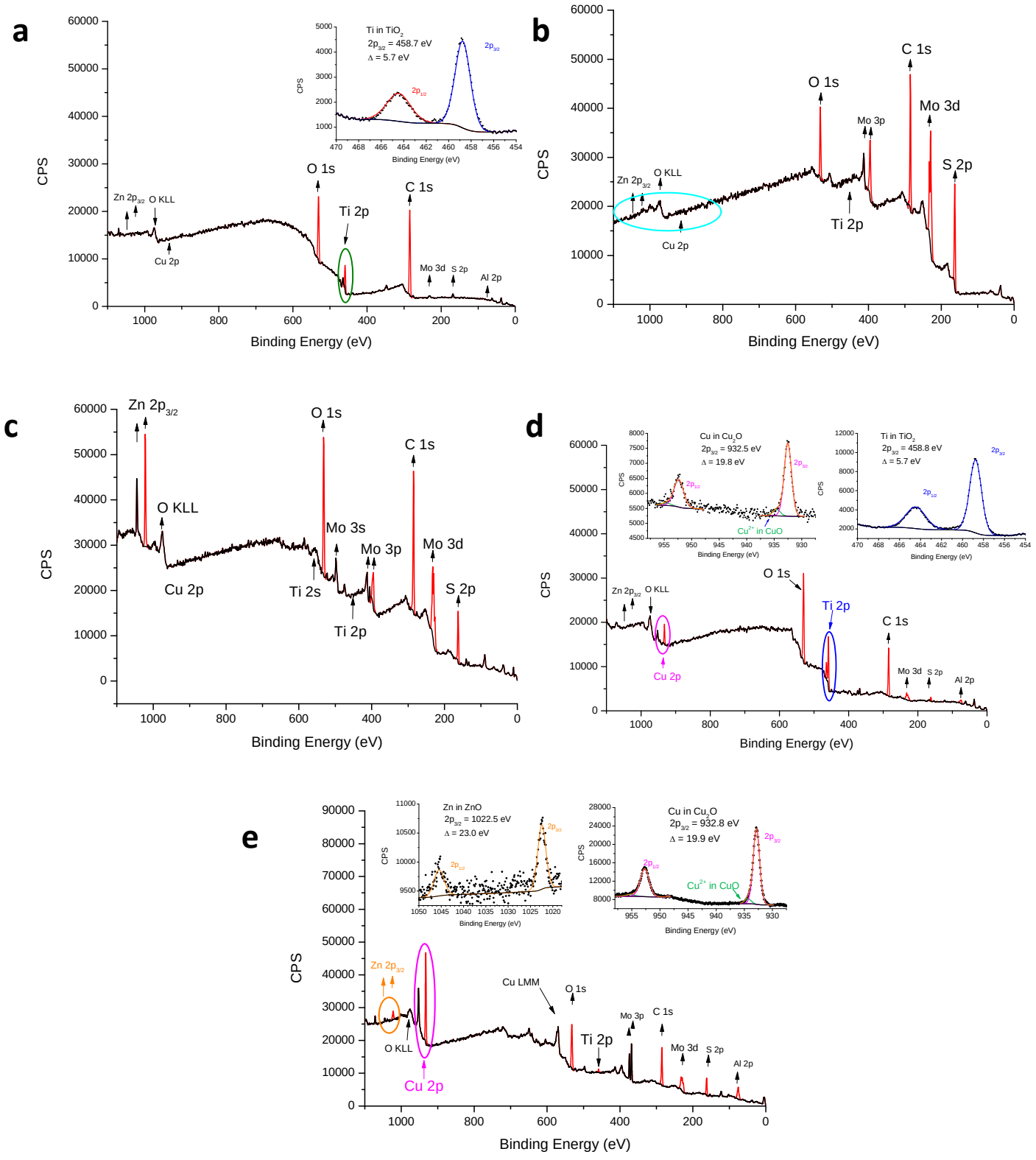

Supplementary Figure 4. Wide-range XPS spectra of the photocathode surface. (a) Surface-protected Cu_2O photocathode without a HER catalyst (Inset: Ti 2p region). **(b)** As-prepared photocathode by constant anodic (MoS_{2+x}-CA-Cu_2O) PEC deposition. The absence of Zn, Cu and Ti peaks indicate a conformal MoS_{2+x} film of at least 10 nm thick. **(c)** MoS_{2+x}-CA-Cu_2O after 1 h of continuous hydrogen production under AM 1.5 illumination at pH 1.0. The presence of Zn peaks and absence of Ti peaks indicate pinholes in the MoS_{2+x} layer where TiO_2 has been etched away. **(d)** Deactivated MoS_{2+x}-CV-Cu_2O after 8 h at pH 1.0 (no remaining photocurrent). Little Mo remains;

Zn is not observed due to the dissolution of the ZnO after prolonged exposure to the acid electrolyte. Insets show that the remaining Ti and Cu are present in the form of TiO_2 and Cu_2O, respectively. The small shoulder at 934.6 eV corresponds to CuO probably formed by exposure of Cu_2O to air before XPS measurements. **(e)** MoS_{2+x}-CV-Cu_2O photocathode after 10 h of testing at pH 9.0 (80% of initial photocurrent remaining). Mo, Zn, Al and Cu are all present.

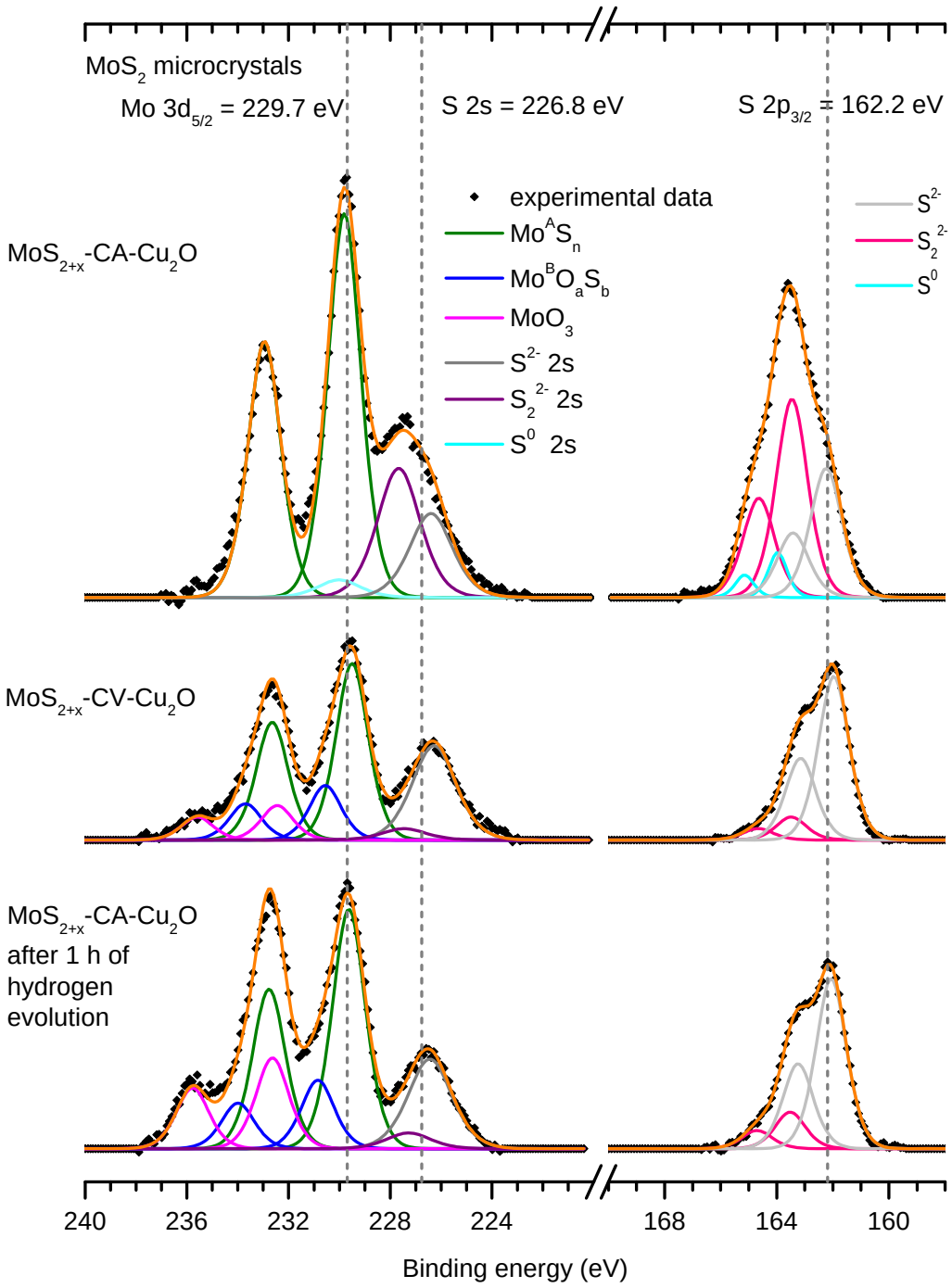

Supplementary Figure 5. XPS characterization of HER catalyst on Cu_2O photocathode. XPS spectra of the photocathode surface as prepared by constant anodic (MoS_{2+x}-CA-Cu_2O) and cyclic voltammetry (MoS_{2+x}-CV-Cu_2O) photo-electrodeposition and MoS_{2+x}-CA after 1 h of continuous hydrogen production under AM 1.5 illumination at pH 1.0. Dotted vertical lines indicate the binding energy of the Mo $3d_{5/2}$, S $2p_{3/2}$ and S 2s components measured for commercially available MoS_2 microcrystals (Aldrich, powder) for comparison.

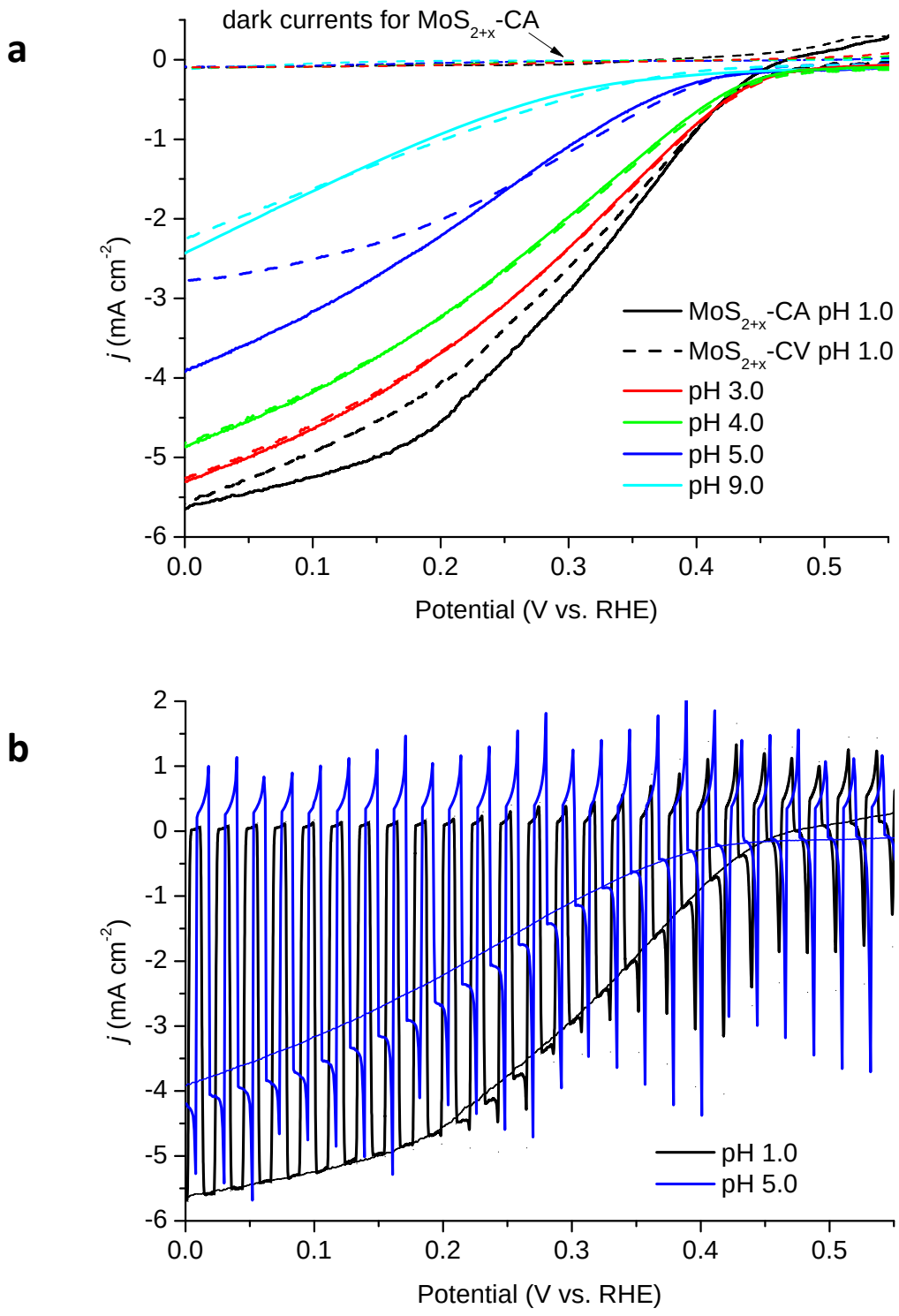

Supplementary Figure 6. Solar driven PEC hydrogen evolution (a) Current-potential curves at different pH values for a MoS_{2+x}-CA-Cu_2O photocathode (10^{th} scan, solid lines). Scan rate is 10 mV s^{-1} in the cathodic direction. Geometric surface area is 0.26 cm^2 and the catalyst loading is 36 μg cm^{-2}. For comparison, the photocurrent dependence on pH for the MoS_{2+x}-CV-Cu_2O photocathode is shown in dashed lines. **(b)** Chopped light photocurrents for the MoS_{2+x}-CA-Cu_2O photocathode at both pH = 1 and 5. A transient behavior was observed at pH 5.0. Photocurrents under AM 1.5 constant illumination are shown as a reference.

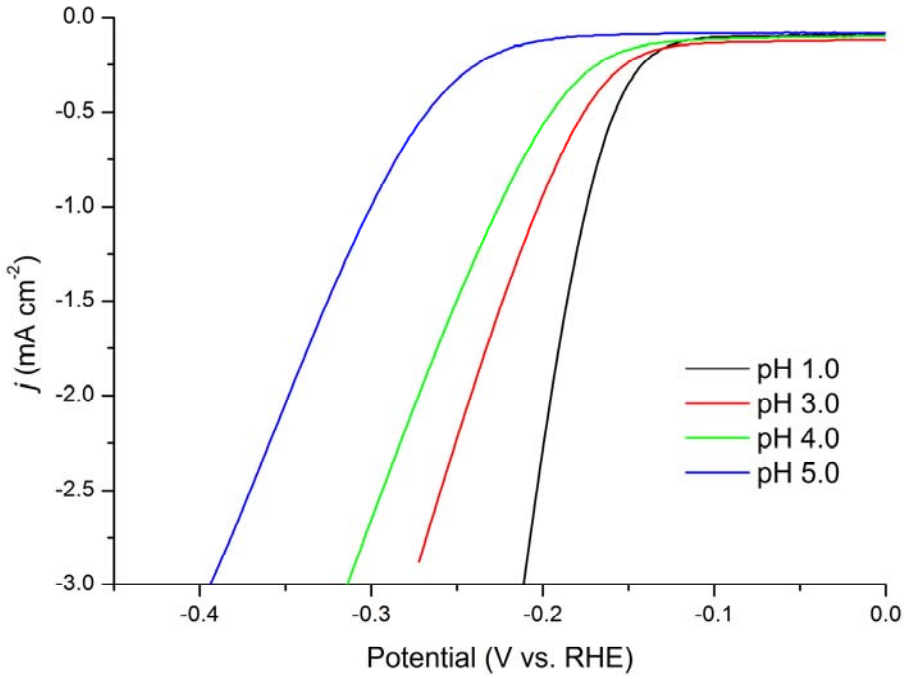

Supplementary Figure 7. Current density versus potential behavior at different pH for a MoS_{2+x} film **grown on FTO** by cyclic voltammetry (50cycles). The deposition method for MoS_{2+x} was previously described by us (Merki et al.[18]). The current densities are not corrected for ohmic resistance.

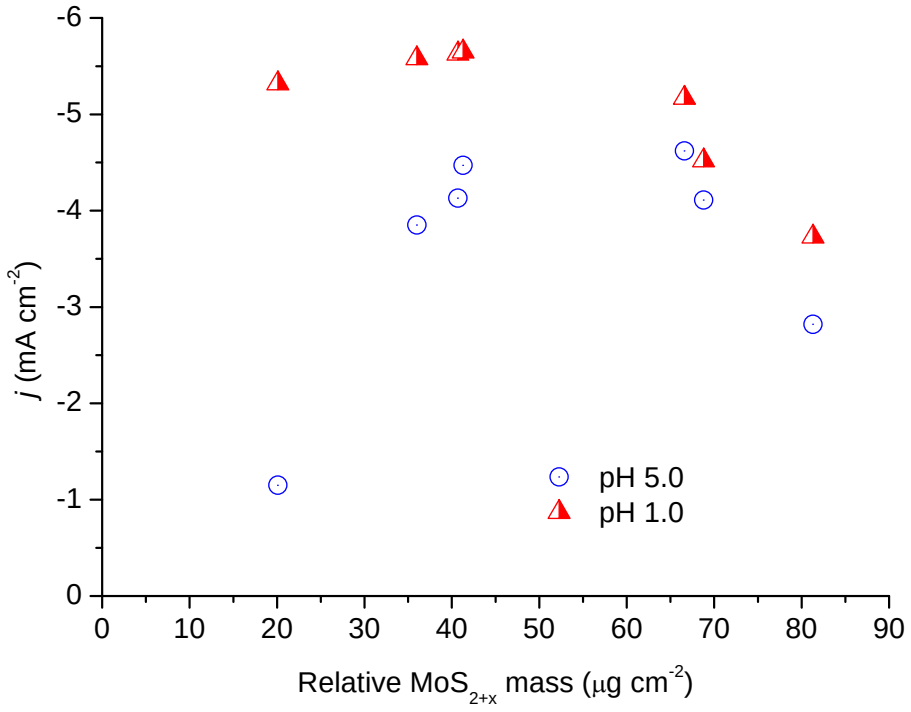

Supplementary Figure 8. Current density at 0 V vs. RHE under AM 1.5 illumination (pH 1.0 and 5.0) for various photocathodes with different MoS_{2+x} catalyst loading deposited by constant anodic photoelectrodeposition (MoS_{2+x}-CA-Cu_2O). The amount of MoS_{2+x} deposited is calculated from the total current passed during PEC deposition assuming a two electron oxidation process from MoS_4^{2-} in solution to MoS_3 + S^0 on the photocathode and knowing that the active HER catalyst is amorphous MoS_2 of molar mass close to 160 g/mol.[20]

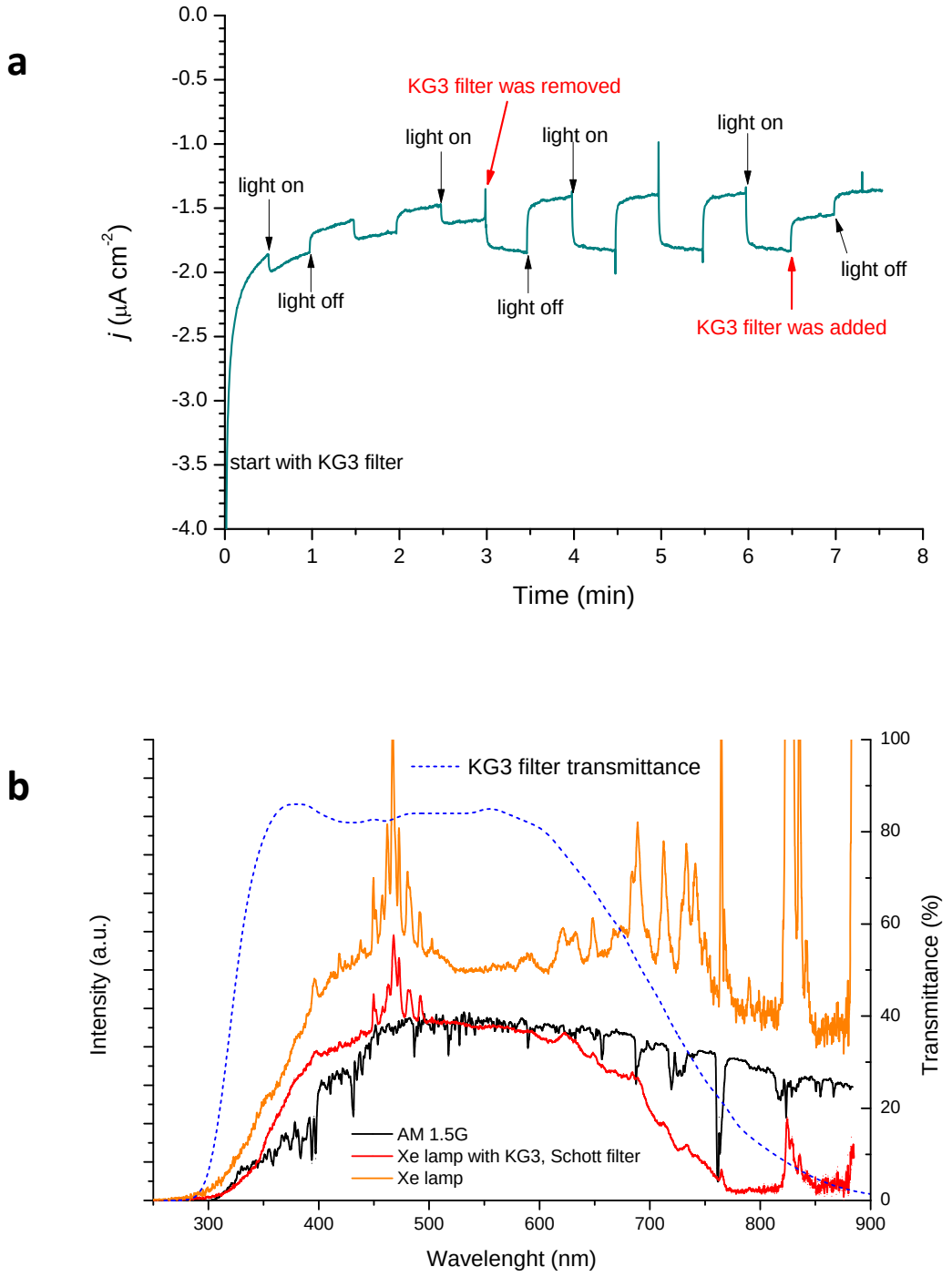

Supplementary Figure 9. (a) Current density versus time behavior in pH 1.0 at 0 V vs. RHE for a MoS_{2+x} film photodeposited by cyclic voltammetry on 100 nm of TiO_2 grown by ALD on FTO. The consecutive changes in photocurrent correspond to the turning on and off (chopping) of the Xe lamp light unless otherwise indicated. Red arrows indicate the addition and withdrawal of the KG3 filter while the light is kept on. **(b)** Irradiance of the Xe light source (using a halogen bulb with a temperature color of 3200K as reference) with and without the use of the KG3 filter. Right axis: light transmittance data of the KG3 filter available from provider.

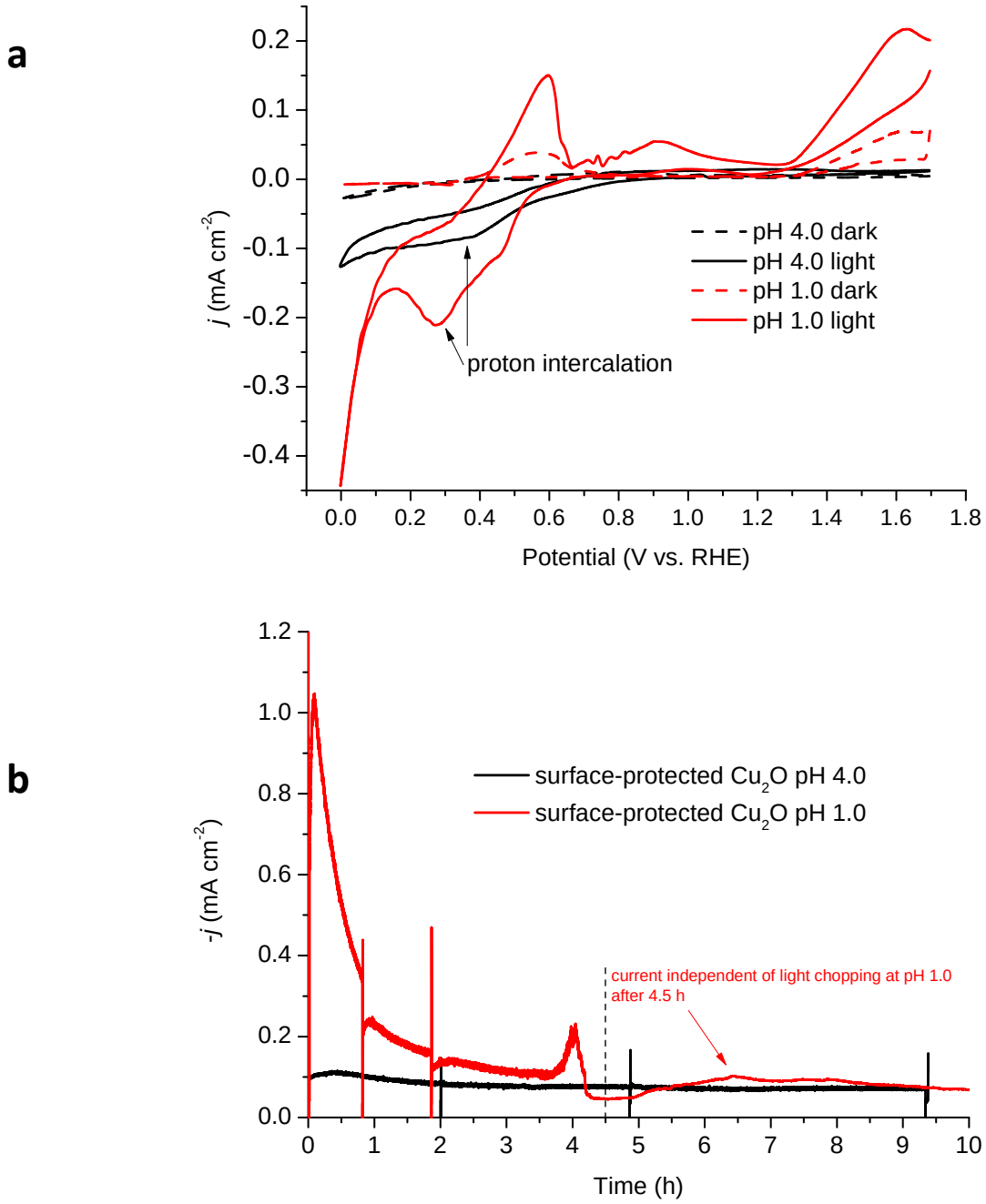

Supplementary Figure 10. Surface-protected Cu_2O without an HER catalyst. (a) Cyclic voltammetry before stability test. A Ti metal wire was used as counter electrode in a three electrode configuration where the potential was swept at 10 mV s^{-1} starting from the most anodic potential. Peaks for proton intercalation in the TiO_2 under light are similar to those reported by Chorkendorff and co-workers for 100 nm ALD TiO_2/5nm Ti on a highly conductive degenerately doped n-silicon in the dark[28]. **(b)** Long term stability under AM 1.5 illumination at different pHs for the surface-protected Cu_2O photocathodes without HER catalyst in (a). The photocathode was biased at 0 V vs. RHE. Periodic chopping of the light source was done to observe dark reductive corrosion of the Cu_2O film. After 4.5 h of testing at pH 1.0, no photocurrent remains and only dark corrosion is observed.

a

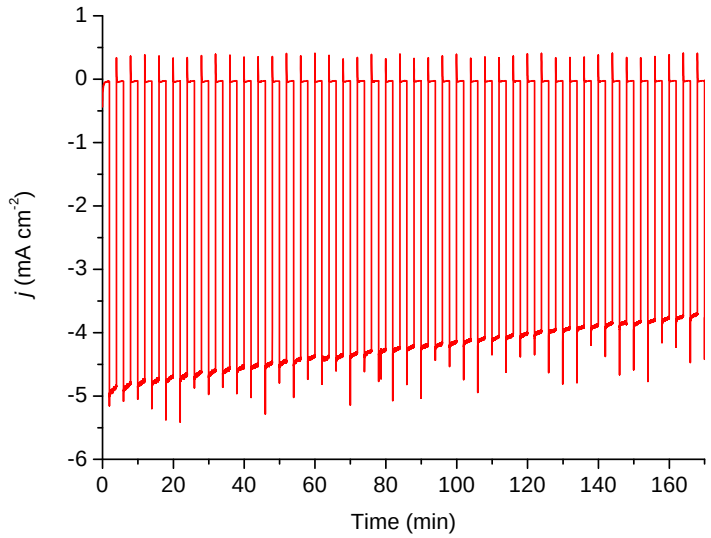

b

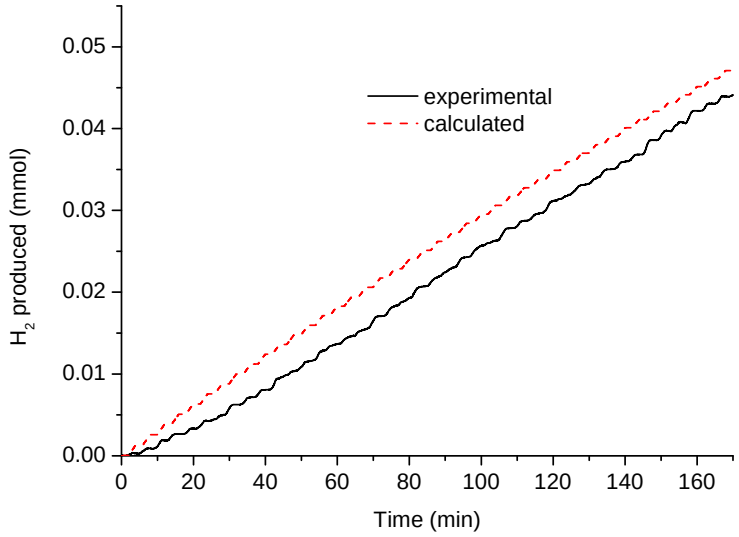

Supplementary Figure 11. Hydrogen production efficiency of a MoS_{2+x}-CA-Cu_2O photocathode held at 0V vs. RHE at pH 4.0 in a closed H shape cell under chopped AM 1.5 irradiation. (a) Time dependence of current density (geometric area = 0.28 cm^2). The small decrease in photocurrent is due to the formation of small bubbles on the photocathode surface and depletion of protons in the electrode vicinity due to the lack of stirring in the closed system. The initial photocurrent is recovered when fresh solution is added and stirred. **(b)** Calculated vs. real hydrogen production. After the induction period of 20 min, the slopes of the experimental and theoretical curves are similar indicating Faradaic efficiency close to 100%. The calculated vs. real hydrogen production after the induction period of 20 min is shown in Figure 4b in the main text.

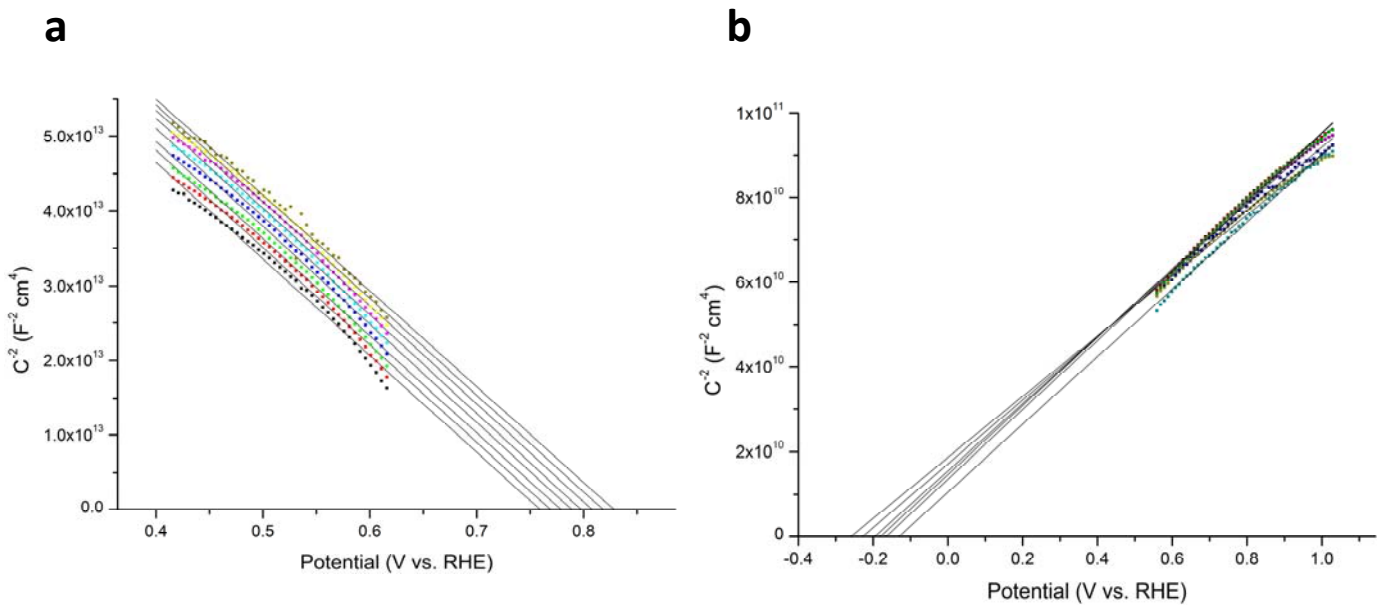

Supplementary Figure 12. Mott-Schottky analysis for the Cu_2O and TiO_2 layers of the device. (a) Cu_2O, pH 7.9 (2-50 Hz). **(b)** TiO_2 (100nm), pH 12.9 (0.2-3 kHz)

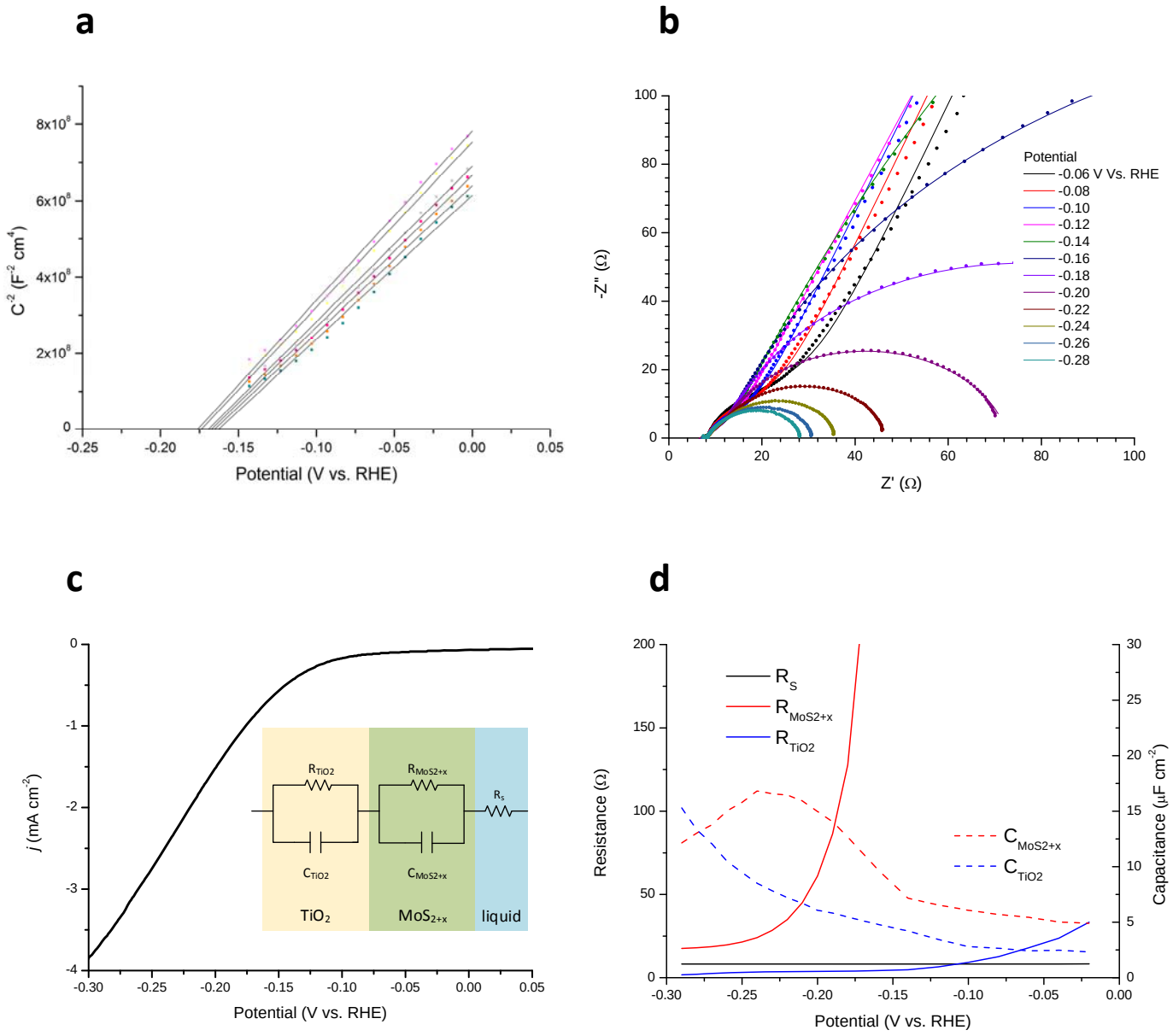

Supplementary Figure 13. Mott-Schottky and Nyquist plot analysis for MoS_{2+x} grown on 100 nm TiO_2. (a) Mott-Schottky plot, pH 1.0 (0.5-1 kHz). **(b)** Nyquist plot. Potential is indicated against the RHE. The pH of the solution is 1.0. **(c)** Potential vs. current density behavior at pH 1.0. Inset: equivalent circuit used to fit the experimental data in (b). **(d)** Charge transfer resistance(**R**) and capacitance (**C**) values calculated for the equivalent circuit in (b).

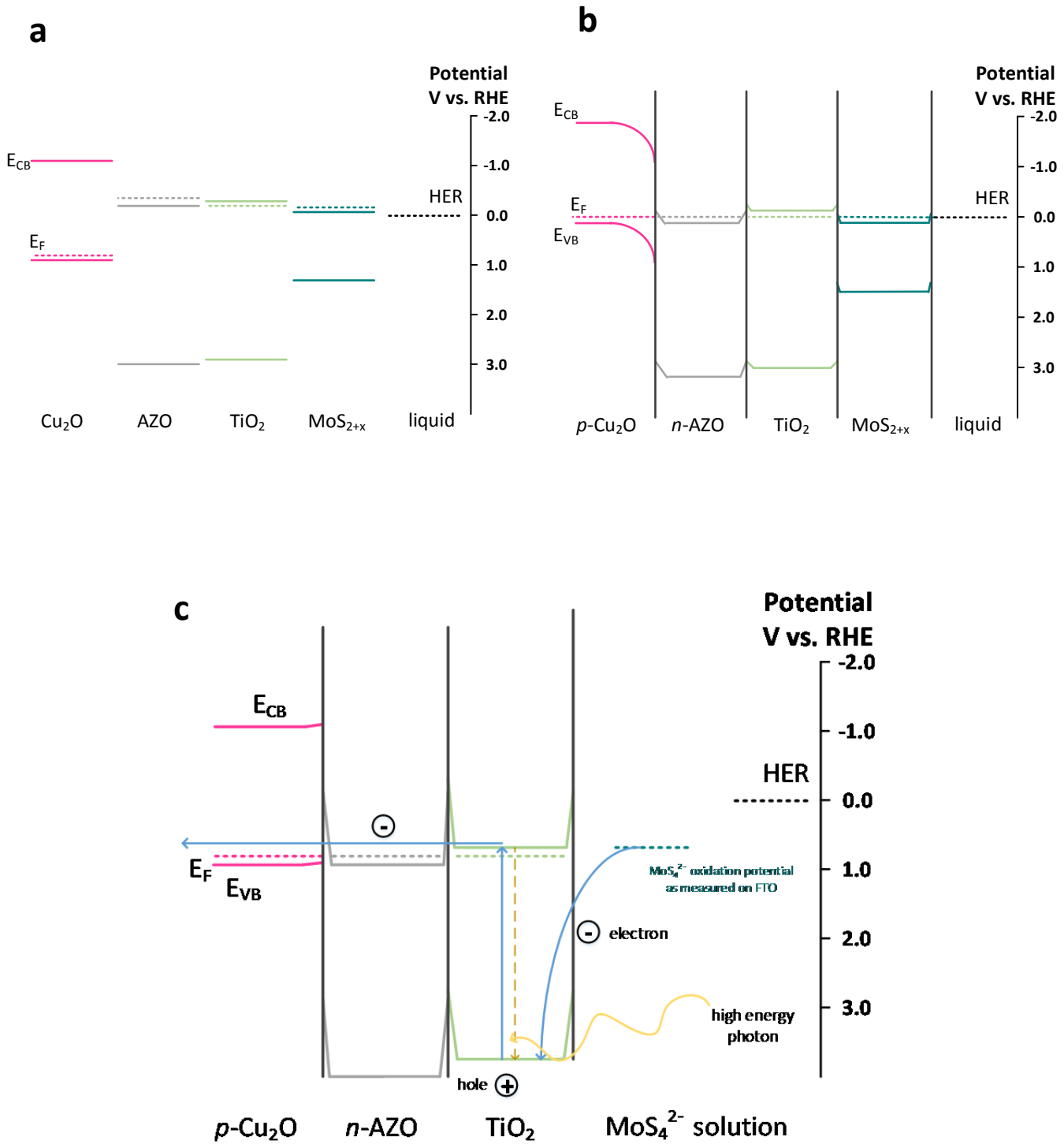

Supplementary Figure 14. Band diagram. For clarity, the x-axes are not to scale. **(a)** Band positions determined by Mott-Schottky analysis. The electrical properties of MoS_{2+x} used in the band diagram are those of MoS_{2+x} on 100 nm TiO_2. **(b)** Equilibrated multijunction in the dark biased at 0V vs. RHE. **(c)** Band positions during MoS_{2+x} catalyst deposition under unfiltered Xe lamp illumination. The photocathode is depicted as biased at +0.81 V vs. RHE. The oxidative deposition of MoS_3 on FTO has been reported to take place when the working electrode is biased to potentials more positive than + 0.7 V vs. RHE.[18,20]

Supplementary Table 1. Binding energy of representative XPS components.

Sample	$Mo^{A}S_n$ $3d_{5/2}$ (eV)	$Mo^{B}O_aS_b$ $3d_{5/2}$ (eV)	Equivalent S 2S singlet (eV)	S^{2-} $2p_{3/2}$ (eV)	S_2^{2-} $2p_{3/2}$ (eV)	S^0 $2p_{3/2}$ (eV)	Mo:S ratio
MoS_2 crystal	229.7		226.8	162.2			1:1.9
MoS_x-CA	229.8		227.5	162.2	163.5	164.0	1:3.4
MoS_x-CV	229.5	230.6	226.3	162.0	163.5		1:2.7
MoS_x-CA-act	229.6	230.8	226.5	162.1	163.5		1:1.9

Supplementary Table 2. Full width at half maximum values used in XPS data fitting and contribution of the different Mo and S components to the total element content.

Sample	Mo 3d FWHM (eV)	S 2s FWHM (eV)	S 2p FWHM (eV)	$Mo^{A}S_n$, $Mo^{B}O_aS_b$, MoO_3 contribution to Mo content (%)	S^{2-}, S_2^{2-}, S^0 contribution to S content (%)
MoS_2 crystal	0.87	1.91	0.84	96, 0, 4	100, 0, 0
MoS_x-CA	1.52	1.98	1.32 S^0 (0.80)	100, 0, 0	36, 56, 8
MoS_x-CV	1.50	2.02	1.28	68, 20, 12	88, 12, 0
MoS_x-CA-act	1.52	2.02	1.28	60, 17, 23	82, 18, 0

Supplementary Table 3. Summary of performance and stability for Cu_2O photocathodes reported by our group.

Reference	Light harvesting material	HER catalyst	*j* at 0 V vs. RHE	Stability* (pH)
This work	Cu_2O/AZO/(100 nm)TiO_2	MoS_{2+x}	-5.7 mA cm^{-2} -4.5 mA cm^{-2} -2.0 mA cm^{-2}	5 h at pH 1 10 h at pH 4 10 h at pH 9
Paracchino et al.[10]	Cu_2O/AZO/(11 nm)TiO_2	Pt	-7.6 mA cm^{-2}	20 min at pH 5
Paracchino et al.[22]	Cu_2O/AZO/(20 nm)TiO_2	Pt	-4.5 mA cm^{-2}	10 h at pH 5 chopped light
This work	Cu_2O/AZO/(100 nm)TiO_2	Pt	-8.0 mA cm^{-2}	2.5 h at pH 1
Tilley et al.[23]	Cu_2O/AZO/(100 nm)TiO_2	RuO_2	-5.0 mA cm^{-2}	8 h at pH 5 chopped light

***** Stability defined as the time when at least 50% of the initial photocurrent value is conserved or the maximum period of test reported.

Supplementary Table 4. Summary of performance and stability for photocathodes made entirely of abundant elements reported to date.

Reference	Light harvesting material	HER catalyst	*j* (0 V vs. RHE)	Stability* at 0V vs. RHE (pH)	Photocurrent onset (vs. RHE)
This work	Cu_2O/AZO/TiO_2	MoS_{2+x}	-5.6 mA cm^{-2} -4.5 mA cm^{-2} -2.0 mA cm^{-2}	5 h at pH 1 10 h at pH 4 10 h at pH 9	0.45 V
Seger et al.[13]	Ti-n^+p-Si	MoS_x	-14 mA cm^{-2}	1 h at pH 0 (+0.2 V vs. RHE)	0.33 V
Tran et al.[34]	Si-nano wires	MoS_2	-1 mA cm^{-2}	1 h at pH 5.0	0.25 V
Hou et al.[11]	Si pillars	Mo_3S_4 cluster	-9 mA cm^{-2}	24 h light/dark cycles at pH 0	0.15 V
Warren et al.[12]	n^+p-Si microwire	Ni-Mo	-9.1 mA cm^{-2}	1 h at pH 4.5	0.46 V
Laursen et al.[17]	n^+p-Si	MoS_2/Mo	-10 mA cm^{-2}	5 d in 1 M $HClO_4$	0.30 V
Laursen et al.[17]	n^+p-Si	MoS_x/MoS_2/Mo	-12 mA cm^{-2}	24 h in 1M $HClO_4$ (+0.2 V vs. RHE)	0.34 V
Bourgeteau et al.[15]	P3HT:PCBM	MoS_x	-0.2 mA cm^{-2}	45 min in H_2SO_4 0.5 M (+0.16 V vs. RHE)	0.50 V
Lin et al.[16]	Cu/nanoCu_2O	NiO_x	-4.98 mA cm^{-2}	20 min (+0.26 V vs. RHE) at pH 6.0	0.46 V
Zhang et al.[14]	C/Cu_2O NWAs/Cu mesh	-	-3.95 mA cm^{-2} (0 V)	1 h in 1 M Na_2SO_4	0.60 V

***** Stability defined as the time when at least 50% of the initial photocurrent value is conserved or the maximum period of test reported.

Supplementary Table 5. Electrical properties of the individual components of the MoS_{2+x}-Cu_2O photocathode.

Layer	E_{fb} (V vs. RHE)	N_A (cm^{-3})	N_V (cm^{-3})	$E_F - E_{VB}$ (mV)
Cu_2O	+0.81	1.6×10^{17}	1.1×10^{19}	100
Layer	E_{fb} (V vs. RHE)	N_D (cm^{-3})	N_C (cm^{-3})	$E_{CB} - E_F$ (mV)
AZO*	-0.33	1.6×10^{21}	3.5×10^{18}	159 (degen.)
TiO_2	-0.20	2.4×10^{19}	7.9×10^{20}	-90
MoS_{2+x} on TiO_2	-0.17	1.2×10^{21}	8.9×10^{18}	127 (degen.)

* Reference 22.

Supplementary Note 1.

XPS Analysis

X-ray photoelectron spectra collected before electrochemical testing for the photocathode prepared by anodic constant voltage photodeposition, MoS_{2+x}-CA-Cu_2O, shows that the as-deposited material resembles molybdenum trisulfide (MoS_3). A model consisting of at least three doublets for the S 2p region was necessary to correctly approximate the S 2p region of the XPS spectra. The three doublets can be attributed to sulfur atoms in multiple oxidation states consistent with previous reports of MoS_3 materials, which contain sulfur in a combination of S_2^{2-} and S^{2-} groups[26] and metallic sulfur S^0.[20] Following the fitting of the S 2p region, three different states of sulfur were also used to fit the S 2s peak in the Mo 3d region keeping the same areas ratio as those of the S 2p peak deconvolution. The use of one equivalent singlet to fit the S 2s region at 227.5 eV is the common approach found in the literature although one S 2s singlet exists for each S 2p doublet.[27] Supplementary Table 1 and 2 summarizes the binding energy for the different components and the full width at half maximum (FWHM) values used in the XPS data fitting. The FWHM were constrained to within 0.05 eV of difference for the three photocathodes measured. One doublet with Mo $3d_{5/2}$ component at 229.8 eV gives a good fit for the Mo peak. This peak can be attributed to Mo^{4+} in MoS_3.[27] The MoS_{2+x}-CA-Cu_2O has an activation process during which less than quantitative amounts of hydrogen are produced (First 20 min in Supplementary Figure 11b) while MoS_{2+x}-CV-Cu_2O is already in the active phase. The XPS spectra for the MoS_{2+x}-CA-Cu_2O after one hour of hydrogen evolution has a S:Mo ratio of 1.9:1 and is similar to that of as-prepared MoS_{2+x}-CV-Cu_2O.[18] At least three doublets are necessary to correctly fit the Mo 3d region for photocathodes MoS_{2+x}-CV-Cu_2O and MoS_{2+x}-CA-Cu_2O after activation. The doublet with higher binding energy and Mo $3d_{3/2}$ component at 235.7 eV corresponds to molybdenum in MoO_3. This MoO_3 can be attributed to air oxidation of the MoS_{2+x} film during transfer of the sample for XPS measurements. The MoO_3 is not observed for the MoS_{2+x}-CA-Cu_2O sample although all samples were similarly exposed to air. These results are in agreement with the nature of the films deposited previously onto Au and FTO electrodes under similar conditions in the dark and indicate that the hydrogen evolution is efficiently catalyzed by amorphous MoS_{2+x} deposited on the Cu_2O photocathode.[20]

A third doublet at 230.7 eV appears for the activated MoS_{2+x} catalyst. This Mo has a binding energy intermediate between that for Mo^{4+} in MoS_3 and MoS_2 and Mo^{6+} in MoO_3 and can be attributed to molybdenum oxysulfide species $Mo^{B}O_aS_b$.[20] The mechanism of formation of the molybdenum oxide and the relation of the $Mo^{B}O_aS_b$ species to the catalytic activity of the amorphous film for H_2 evolution is of high interest and more thorough studies are necessary.

Supplementary Note 2.

Mott-Schottky Analysis

The donor density, N_D, was calculated from the slopes of the Mott-Schottky plots by the following equation where A_s is the geometric surface area of the measured sample using dielectric constants (ε) of 6.6 for Cu_2O[29], 75 for TiO_2[30] and 28 for MoS_2[31].

$$\frac{1}{C^2} = \frac{2}{e\varepsilon\varepsilon_0 N_D A_s^2}\left(E - E_{fb} - \frac{kT}{e}\right)$$

The calculated N_D values were used to calculate the difference between the conduction band and the Fermi level using:

$$E_{CB} - E_F = \frac{kT}{e} ln\left(\frac{N_C}{N_D}\right)$$

The values for the effective density of states in the conduction band, N_C, were calculated using an electron effective mass (m^*) of 0.58 m_0, 10 m_0 and 0.5 m_0 for Cu_2O, TiO_2 anatase and MoS_2, respectively in the equation $N_C = 2\left(\frac{2\pi m^* kT}{h^2}\right)^{3/2}$.

The depletion width in the junction between the p-type Cu_2O and the n-type AZO can be calculated using the respective following equations:

$$w_p = \sqrt{\frac{2\varepsilon_0\varepsilon_p(N_D \cdot \varepsilon_n)}{eN_A(N_A \cdot \varepsilon_p + N_D \cdot \varepsilon_n)} \cdot V_b}$$

$$w_n = \sqrt{\frac{2\varepsilon_0\varepsilon_n(N_A \cdot \varepsilon_p)}{eN_D(N_A \cdot \varepsilon_p + N_D \cdot \varepsilon_n)} \cdot V_b}$$

Where ε_p and ε_n are the relative dielectric constants ($\varepsilon_p = 6.6$ for Cu_2O[29] and $\varepsilon_n = 3.8$ for ZnO[32]), $N_A = 1.6 \times 10^{17}$ and $N_D = 1.6 \times 10^{21}$ are the acceptor and donor concentrations from Supplementary Table 5 and V_b is the built-in potential, which, to a first approximation, is taken to be equal to the flatband position difference for Cu_2O

and the AZO layer. Thus, according to the Mott-Schottky analysis, $V_b = 1.14\,V$ and $w_p = 71\,nm$ and $w_n < 0.1\,nm$. Experimentally, however, the built-in potential has been found to be between 0.5 and 0.6 V, indicating that $w_p \approx 50\,nm$. The depletion width in the Cu_2O photoabsorber (w_p) in both cases is short compared to the Cu_2O film thickness of 400 nm and thus band bending at the interfaces is possible. The high doping of the AZO, TiO_2 and MoS_{2+x} layers corresponds to a depletion width in the order of few atom layers.

Supplementary Table 5 summarizes the electrical properties of the individual layers obtained through the Mott-Schottky analysis shown in Supplementary Figures 12 and 13.

Supplementary Fig. 13 shows the Mott-Schottky and Nyquist analysis for MoS_{2+x} deposited on 100 nm of TiO_2 grown on FTO. The PEC deposition of MoS_{2+x} was carried under the same conditions for MoS_{2+x}-CV-Cu_2O as indicated in the Methods section of the main text.

The potential-current density plot in Supplementary Fig. 13c shows that the evolution of hydrogen requires overpotentials of at least 130 mV. This indicates that the slopes of the Mott-Schottky plot in Supplementary Fig. 13a correspond to the MoS_{2+x} film during depletion. The flat band potential and donor density are summarized in Supplementary Table 5. The high donor density of this n-type semiconductor (~10^{21} cm^{-3}) is two orders of magnitude higher than that of the TiO_2 layer grown by ALD (~10^{19} cm^{-3}).

Two semicircles are observed in the Nyquist plot in Supplementary Fig. 13b as expected for the two layers of the device. The small semicircle at higher frequencies corresponds to the charge transfer resistance through the TiO_2 film, R_{TiO2}, which is small (<30 Ω) in the range of potential analyzed here. The charge transfer resistance of the TiO_2 layer (R_{TiO2}) is small and decreases at higher overpotential. The second semicircle at lower frequencies is related to the kinetics of MoS_{2+x} electrocatalysis. A lower value for R_{MoS2+x} corresponds to a faster reaction rate. R_{MoS2+x} depends strongly on overpotential (Supplementary Fig. 13d). At η = 140 mV, R_{MoS2+x} is higher than 1000 Ω. However, R_{MoS2+x} decreases at higher overpotentials. At η = 200 mV, R_{MoS2+x} falls below 60 Ω in agreement with previous results for MoS_{2+x} deposited directly on FTO[33]. With values between 8 and 9 Ω, the uncompensated solution resistance R_s is low. As expected, this resistance is overpotential independent.

Supplementary References

26 Weber, T., Muijsers, J. C. & Niemantsverdriet, J. W. Structure of amorphous MoS_3. *J. Phys. Chem* **99**, 9194-9200 (1995).

27 Benck, J. D., Chen, Z., Kuritzky, L. Y., Forman, A. J. & Jaramillo, T. F. Amorphous molybdenum sulfide catalysts for electrochemical hydrogen production: Insights into the origin of their catalytic activity. *ACS catal.* **2**, 1916-1923 (2012).

28 Seger, B. *et al.* Silicon protected with atomic layer deposited TiO2: durability studies of photocathodic H2 evolution. *RSC Advances*, doi:10.1039/c3ra45966g (2013).

29 Heltemes, E. C. Far-infrared properties of cuprous oxide. *Phys. Rev.* **141**, 803-805 (1966).

30 King, D. M., Du, X., Cavanagh, A. S. & Weimer, A. W. Quantum confinement in amorphous TiO_2 films studied via atomic layer deposition. *Nanotechnology* **19**, 445401 (2008).

31 Anand, T. J. S. & Shariza, S. A study on molybdenum sulphoselenide thin films: Growth from solution and its properties. *Electrochim. Acta* **81**, 64 - 73 (2012).

32 Noh, H., Scharrer, M., Anderson, M. A., Chang, R. P. H. & Cao, H. Photoluminescence modification by a high-order photonic band with abnormal dispersion in ZnO inverse opal. *Phys. Rev. B* **77**, 115136 (2008).

33 Merki, D., Vrubel, H., Rovelli, L., Fierro, S. & Hu, X. Fe, Co, and Ni ions promote the catalytic activity of amorphous molybdenum sulfide films for hydrogen evolution. *Chem. Sci.* **3**, 2515-2525 (2012).

34 Tran, P. D. *et al.* Novel assembly of an MoS_2 electrocatalyst onto a silicon nanowire array electrode to construct a photocathode composed of elements abundant on the earth for hydrogen generation. *Chem. Eur. J.* **18**, 13994-13999 (2012).